JOURNAL OF THE CANADIAN SOCIETY OF EXPLORATION GEOPHYSICISTS
VOL. 22, NO. 1 (DEC. 1986) P. 73-86

TOMOGRAPHY-BASED IMAGING OF A HEAVY OIL RESERVOIR USING WELL-LOGS, VSP AND 3-D SEISMIC DATA

ROBERT R. STEWART[1] and STEPHEN K.L. CHIU[2]

ABSTRACT

Integrating various data sets to provide one optimal subsurface image is a major goal of the geophysicist. This paper describes a heavy oil Glauconite sandstone development region in southern Alberta and a suite of geophysical measurements made to delineate the structure and stratigraphy of the hydrocarbon reservoir. The results of conventional processing of well-logs, Vertical Seismic Profile (VSP) and 3-D seismic data acquired in this region show the Glauconite sandstone with a dune-like, NNW-SSE trend underlain by the Mississippian and Wabamun carbonates. There is up to 20 m relief on the top of the sandstone in the vicinity of the wells under consideration. The major objective of this paper is to describe the application of a seismic tomographic technique (traveltime inversion - Chiu and Stewart, 1986) and associated procedures which allow the well-logs, VSP and surface seismic data to be processed simultaneously. Initially, a two- or three-dimensional velocity model in depth is constructed by using the well-logs and preprocessed VSP and surface data. Events times are then picked on the VSP and surface data. Rays are iteratively traced through an updated model until convergence of observed to calculated traveltimes is achieved. The result of the tomographic analysis in this case is a two-dimensional velocity structure of the subsurface across the sandstone. The tomographic velocity structure is used as a basis for the conventional VSP/CDP mapping process as well as the 3-D seismic migration. The 3-D seismic and VSP images are found to be quite similar around the well. The time-domain migrated section is converted to a pseudo-sonic log section by using a maximum-likelihood inversion process (Hampson and Russell, 1985) with the tomographic velocities as a constraint. The pseudo-sonic section in time is mapped into depth, once again by using the tomographic velocities. This pseudo-sonic section in depth gives structure on the top of the Glauconite consistent with that of other wells drilled in the area. Previous structure maps derived from well-logs and 3-D seismic data appear to have seriously overestimated the topography of the Glauconite top.

INTRODUCTION

For reservoir development and production purposes, it is important (desirable) to have a section or reservoir map as highly accurate and resolved as possible. Many development areas have had numerous geophysical measurements acquired including well logs, Vertical Seismic Profiles (VSP) and 3-D seismic. These data are all routinely, and usually separately, processed to construct slices or cross-sectional pictures of the reservoir. Several authors (Gaiser *et al.*, 1984a; Omnes, 1984; Pullin *et al.*, 1986) have discussed ways of combining or correlating these data sets (for example, the shaping of surface seismic data at the well location to the VSP at the same well). Because these numerous data sets, acquired in a given area, are often available and then somehow correlated, it is reasonable to attempt to process *them in a simultaneous, optimal fashion.* One method of accomplishing this goal is via seismic tomography. Seismic tomography means, in broad terms, the making of a picture of a slice of the earth, using seismic energy (McMechan, 1983; Worthington, 1984; Stewart, 1985a). In current practice, the term seismic tomography is used somewhat loosely to describe traveltime or amplitude inversion and other full waveform inversion techniques that attempt to reconstruct an accurate picture of some subsurface parameter. Tomographic techniques have been very successfully applied in diagnostic medicine (Seeram, 1983; Censor, 1983; Louis and Natterer, 1983; Morgan, 1983; Roth, 1984). This example has not been lost on geophysicists (*e.g.* Dines and Lytle, 1979; Mason, 1981; Devaney, 1984; Stork and Clayton, 1985) who are attempting to apply these and similar techniques to geophysical problems. Geophysical problems ranging from x-ray tomographic scanning of rocks (G. Sedgwick, *pers. comm.*, 1985) and permafrost delineation (Bishop *et al.*, 1985) to whole earth imaging (Anderson and Dziewonski, 1984) have been treated by tomographic techniques.

Cross-hole (between two wells) tomography has received considerable attention in the literature (Bois *et al.*, 1972; Wong *et al.*, 1983; Peterson *et al.*, 1985; Bregman,

[1]Veritas Software Ltd., 615 - 3rd Avenue S.W., Calgary, Alberta T2P 0G6
[2]Alberta Research Council, 6815 - 8th Street N.E., Calgary, Alberta T2E 7H7

The authors would like to express their appreciation to AEC Oil & Gas Co. and Westcoast Petroleum Co. for releasing the field data used in this paper. *In particular, we would like to thank Keith Young and Andy Mah of AEC for their support of this research and involvement in the* interpretation of the results. Dwight Mildenberger, Bernie Law and Murray Desiarlais assisted in the data processing. Anne Furlotte and Irene Chan patiently typed (and retyped) this manuscript.

1986). At present cross-hole data sets are not commonly acquired. When cross-hole measurements are made in conjunction with surface receivers, though, the possibility of making images of quality approaching that of the medical case exists. The VSP, however, is becoming more and more of a conventionally acquired data set. A VSP survey provides an unambiguous velocity structure in depth and can also be used for lateral imaging. The VSP usefulness is nonetheless restricted by its limited lateral coverage.

Surface data, on the other hand, are routinely acquired and provide broad lateral coverage. But surface seismic sections are generally plagued with at least some ambiguity when converted to depth sections. As wells are drilled in depth and not two-way traveltime, increasing confidence in depth sections is a desirable goal. Coupling VSP and surface data should provide a better (less ambiguous) subsurface picture. In fact, as shown in synthetic studies, this is the case (Chiu and Stewart, 1986). Bregman (1986) demonstrated similar results in great detail via eigenvalue analysis: that adding VSP data to cross-hole data allowed a much better determined and resolved image to be created. The main goal of this study is to apply tomographic techniques and processing flows to the simultaneous (coupled) analysis of well-log, VSP and surface data. In particular, the tomographic technique is used to map the top of a productive heavy oil reservoir (Glauconitic sand) and its neighbouring stratigraphic units.

Geology and Data Acquisition

The area of development interest discussed in this paper is a Cretaceous Glauconitic sandstone reservoir in southern Alberta (Taylor, 1984; Tilley and Longstaffe, 1984) at a depth of about 900 m. This heavy-oil saturated reservoir lies above a Mississippian carbonate unconformity and below a continental sequence of sandstones, shales and coal. The stratigraphic column is shown in Figure 1. The sandstone reservoir of this type is interpreted to be a barrier island deposit or an almost dune-like development cut by silt-filled channels (Tilley and Longstaffe, 1984). The Glauconitic sandstone unit can be in excess of 45 m thick in some regions and is capped by impermeable shales and coals. In addition, a number of observations (such as apparent juxtaposition of different facies in neighbouring wells) suggest that deep faulting occurred during the Mannville deposition. This can explain the occurrences of the thick sandstone sequences. An east-west seismic section (Line 89) is shown in Figure 2. The Glauconitic sandstone is interpreted as the trough at about 850 ms. The Mississippian unconformity is evidenced by the event at approximately 910 ms. The Wabamun event near 960 ms is another strong seismic reflector. A subsea structural contour map of the top of the Glauconitic sandstone is shown in Figure 3 (to be discussed later). Annotated on this map are the main wells used in this study. Total relief of the sandstone from the map is up to approximately 40 m. The trend of the sandstone barrier island or bar is roughly perpendicular to the direction of the wells D, C, B. A number of wells have been drilled in the area, generally just penetrating the sandstone unit. The wells discussed in this paper are currently productive, with production rates and produced volumes dependent on the detailed stratigraphy of the location.

Various well-log measurements were made in selected wells. The wells (B, C, D, 2F, 3F, F2) used in this study had accompanying sonic and/or density logs. Four VSP surveys and one check shot survey were also conducted (see Fig. 4 for a detailed schematic of well and VSP source locations). All surveys used a P wave vibrator source and a wall-clamped, downhole vertical geophone. Wells 3F and F2 had zero offset VSP surveys conducted while well C had two offset VSP surveys and a check shot survey acquired. The VSP source locations for the well C surveys (the main well of interest) were 610 m East and 610 m west of well C, while the check shot source was 25 m north. The west offset VSP had downhole measurements acquired from 895 m to 205 m at 15 m intervals. The east offset VSP had a smaller region of acquisition — 895 m to 610 m at 15 m intervals. There were also seven check shots in Well C

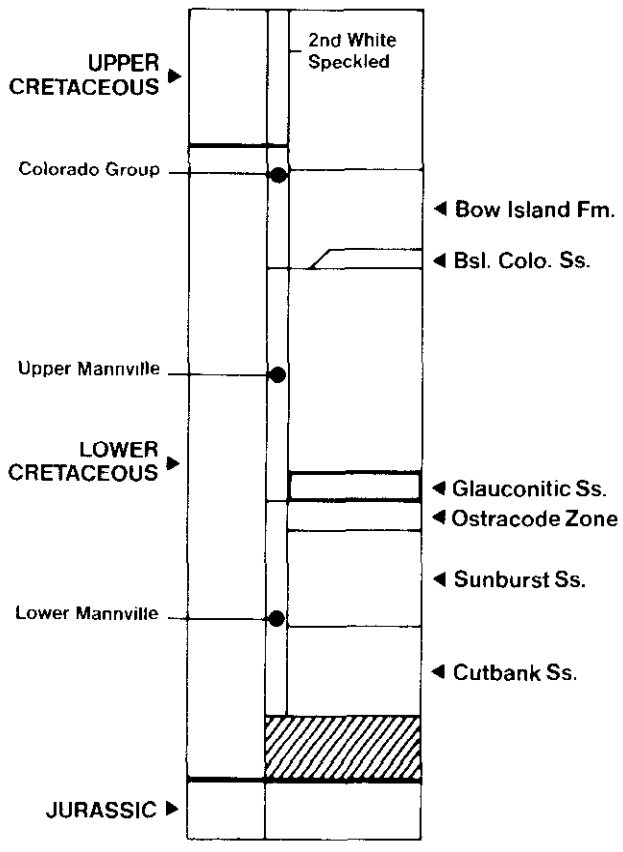

Fig. 1. Stratigraphic chart of southern Alberta Cretaceous geology (after Tilley and Longstaffe, 1984).

separated by about 100 m starting at 907 m and ending at 185 m. Borehole seismic data for well C are shown in Figure 5. Several events (primary and converted waves) are interpreted on the data. It is interesting to note that the P wave vibrator source is offset from the well only 610 m, yet there is a great assortment of wave types propagating in the subsurface.

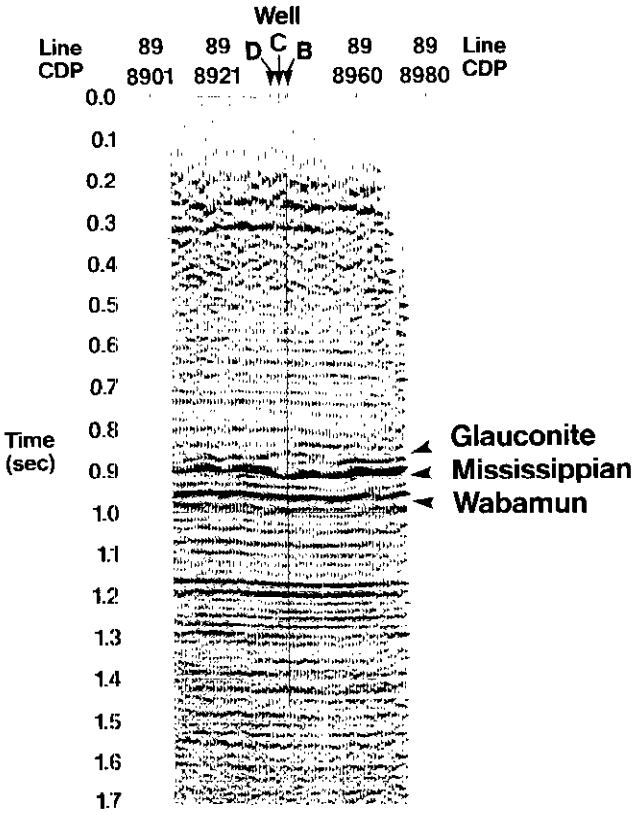

Fig. 2. Single seismic section (Line 89), from a 3-D seismic survey, running perpendicular to the trend of the Glauconitic sandstone. The three major events of interest are annotated.

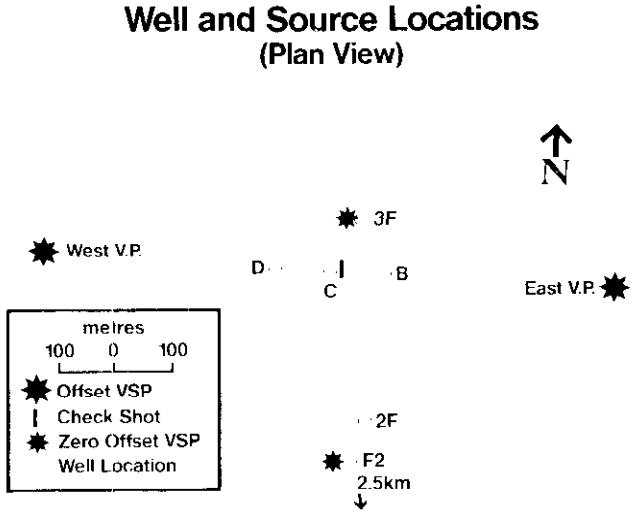

Fig. 4. Well and VSP source locations. Wells B, C, D, 2F and 3F are drilled near the apex of the sandstone trend. Well F2, 2.5 km to the south, is also on the apex of the sandstone trend.

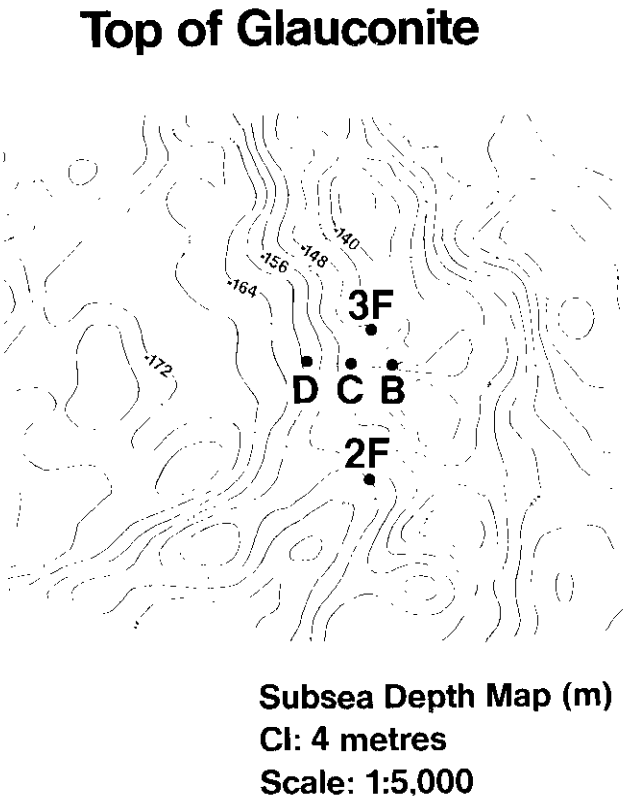

Fig. 3. Plan-view depth map (sub-sea) to the top of the Glauconitic sandstone. Relevant well locations are annotated.

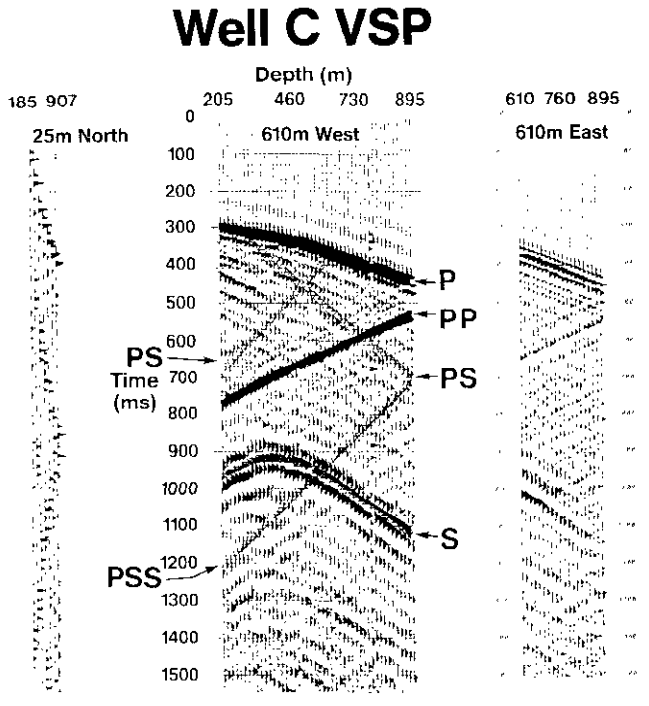

Fig. 5. (a) Check shots (trace equalized) recorded in well C from a P wave vibrator located 25 m to the north of the well. (b) Raw VSP data (trace equalized) recorded in well C from a P wave vibrator offset 610 m to the west of the well. (c) Raw VSP data (trace equalized) recorded in well C from a P wave vibrator offset 610 m to the east of the well.

Figure 6 displays zero offset borehole seismic data acquired in wells F2 and 3F. The VSP in well F2 was acquired over depths 910 m to 410 m at 20 m increments. The high-frequency wave train evident at 910 m depth and time about 0.7 s extending to 1.1 s at 410 m depth is a tube wave bouncing up from the bottom of the well. Various multiple tube waves are also discernible (*e.g.* 1.5 to 1.7 sec). The limited VSP in well 3F was acquired over the depths 910 m to 730 m at 20 m increments with a check shot at 600 m. This VSP was originally shot with the intention of predicting a sonic log below the bottom of the well, but will be used here as a measure of the reflectivity structure near the borehole bottom. The sonic logs for wells 2F and 3F are shown in Figure 7. Both logs just penetrate (by several metres) the top of the Glauconitic sand. The top of the Mannville Group is at about 850 m. The significant velocity decrease below 900 m is evidence of the Glauconitic sand. Gamma ray and density logs from wells D, C and B are displayed in Figure 8. These three logs are shifted to the same datum. The Glauconite is picked on these logs just below 900 m where the density and gamma logs show a marked decrease. Note that there is about a 5 m rise in the Glauconite top from well D to well B.

The sonic and density logs in time from well F2 (2.5 km to the south but also drilled on the sandstone apex) are displayed in Figure 9. Note again, the significant velocity and density decrease at about 355 ms. This bulk-shifted time corresponds to the top of the Glauconite at a depth of 922 m in this well. The synthetic seismograms show a well-developed trough at the Glauconite top.

A 3-D seismic survey was acquired over an area including the region spanned by the well C surveys. Vibrator points were located along N-S lines, shooting into 240 receiving geophones rolled along lines oriented about 15° E-NE. The 3-D source/receiver geometry was such that traces were stacked into 40 m x 40 m bins (CDP bins) giving at least 24-fold stacked traces. Two lines (88 and 89) are used in this study. These lines had been processed previously but were reprocessed with the tomographic velocities. The two final migrated sections proved to be very similar in structure but there was a 90° phase rotation applied to the previously processed data.

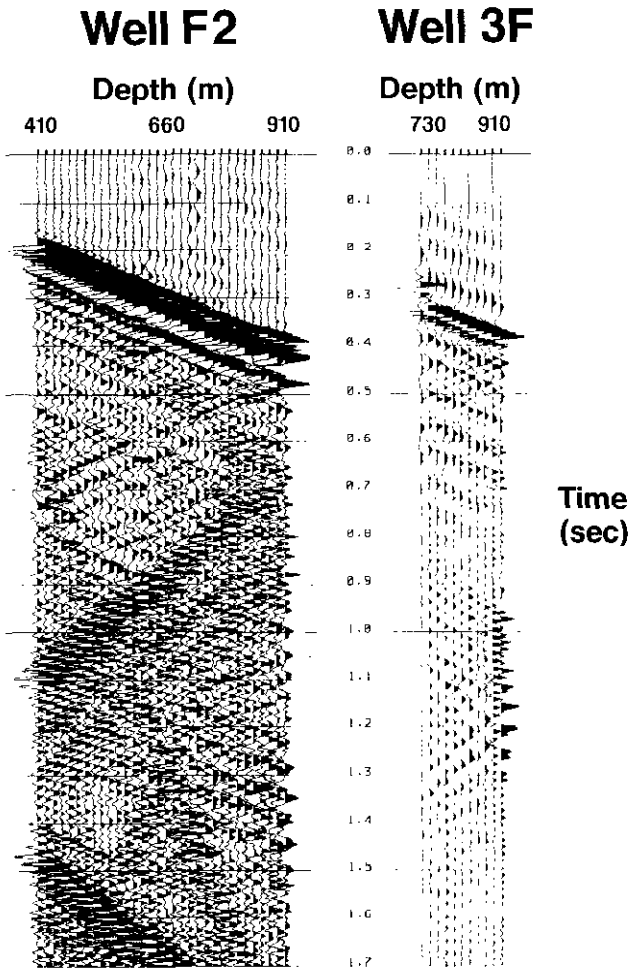

Fig. 6. (a) Raw VSP data (trace equalized) recorded in well F2 from a zero offset P wave vibrator. (b) Raw VSP data (trace equalized) recorded in well 3F from a zero offset vibrator.

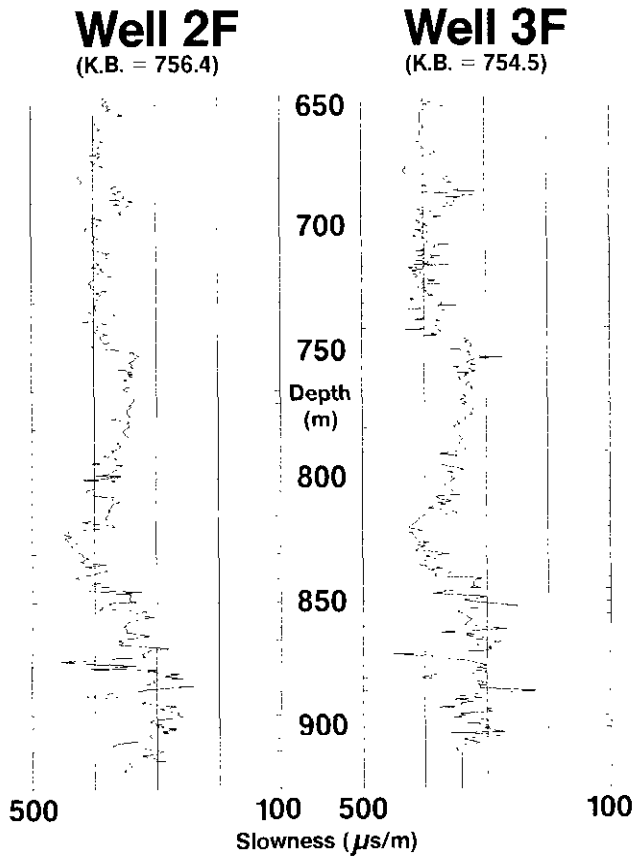

Fig. 7. Sonic logs for wells 2F and 3F. Both logs just penetrate the Glauconitic sand. The similarity of the logs suggests that there is little lithologic change parallel to the trend of the sandstone.

CONVENTIONAL ANALYSIS

The first-break traveltimes from the offset VSP surveys and check shots in well C (Fig. 5) were picked using an interactive computer program. These traveltimes were then inverted separately using an iterative ray-tracing based inversion (Stewart, 1984) to provide a seismic interval velocity versus depth (Fig. 10). The VSP-determined interval velocities versus depth terminate near the top of the Glauconitic sand (at 906 m) in well C. As there were no observations in the top 185 m of the section, this interval was kept at a fixed velocity of 1785 m/s in all inversions. The velocities from the three different surveys are fairly consistent in the deeper part of the section. In the shallow section, there appear to be some notable differences. Some of these differences can likely be attributed to the varying levels of receiver coverage, possible lateral velocity variations and noise. However, looking more closely at the differences between vertical traveltimes from the west offset-determined velocities and the check shot traveltimes, there appears to be a consistent trend (see Fig. 11). At

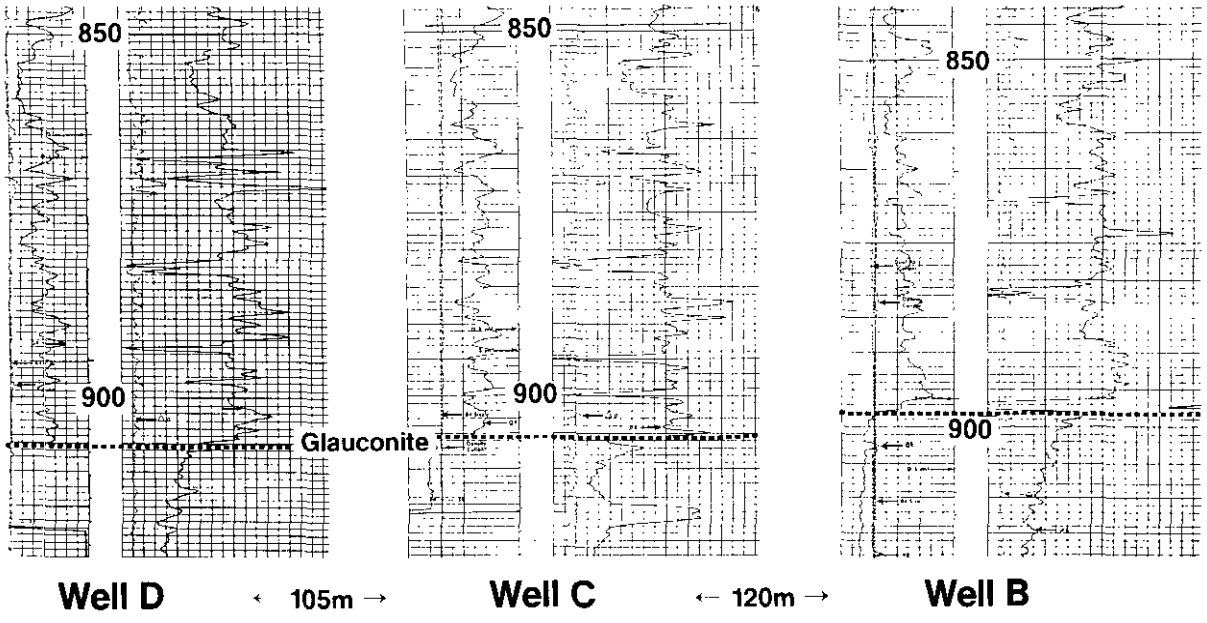

Fig. 8. Gamma ray and density logs for wells D, C and B. Note that there is only about a 5 m rise in the Glauconitic sand top from well D to well B.

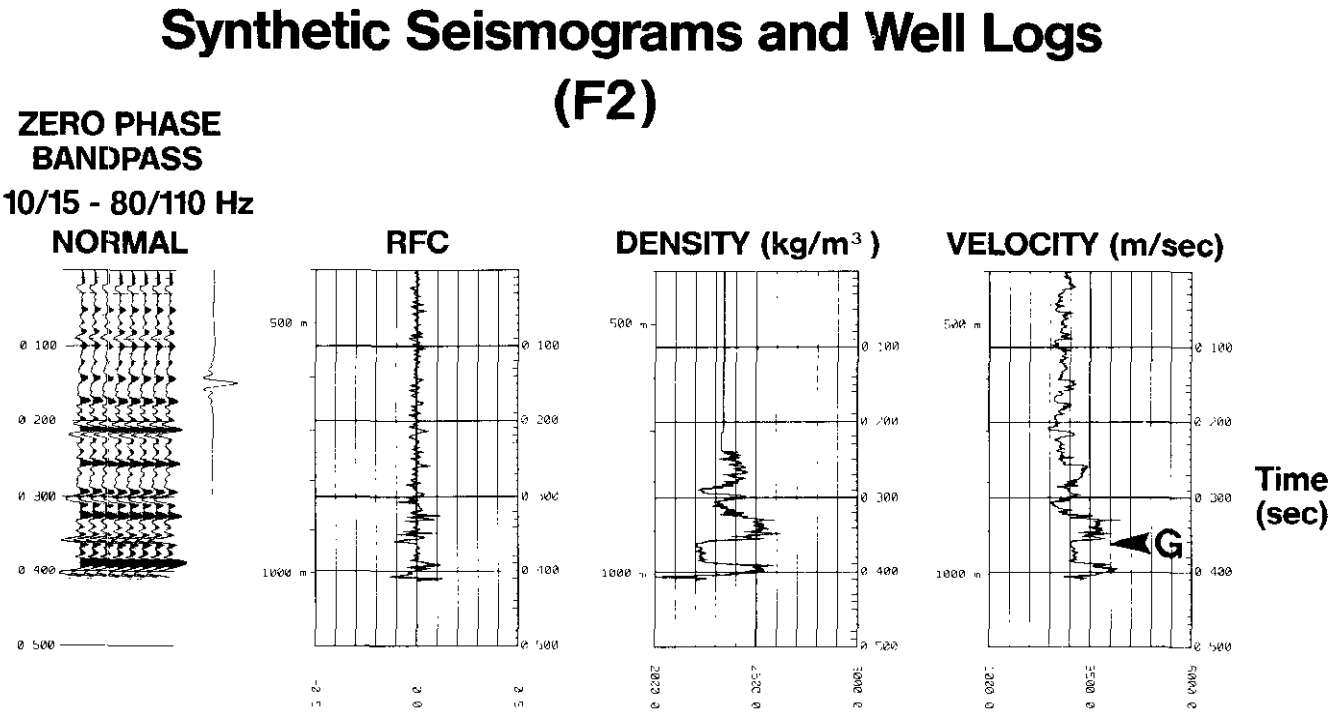

Fig. 9. Well logs and synthetic seismograms from well F2. Note the Glauconitic sand at the bulk-shifted time value below 922 m depth.

greater angles of incidence the offset-determined velocities are higher than the zero offset velocities. More directly, the check shot traveltimes are longer than the vertically incident traveltimes through the offset-determined velocities. Those observations are consistent with the effect of velocity anisotropy (transverse isotropy) to be discussed later. For this reason, rays that had angles of incidence greater than 35° were not used in the conventional P wave analysis.

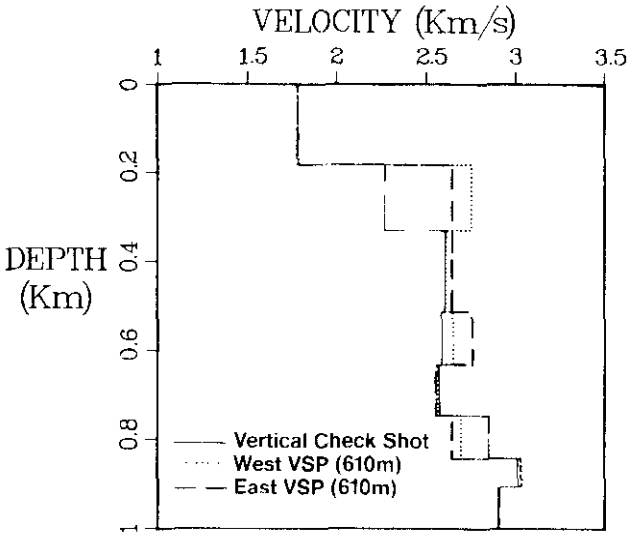

Fig. 10. VSP interval velocities versus depth of Well C VSP data from traveltime inversion of the two offset VSP first-break surveys and check shot survey

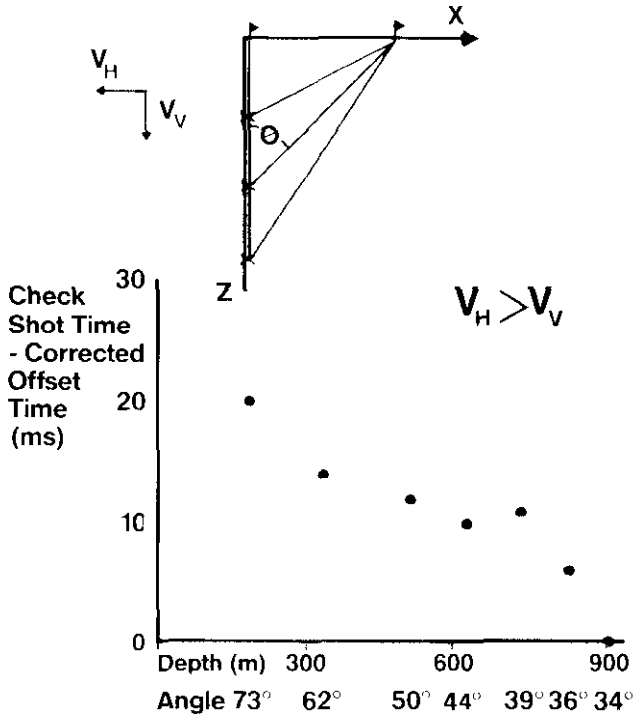

Fig. 11. Check shot times versus offset VSP times corrected to the vertical. The first-break times from the west VSP have been corrected to vertical incidence times using ray trace inversion. These corrected times are shorter than the check shot times to the same depths

Another event of considerable magnitude is visible in the west well C VSP data (Fig. 5) with an arrival time apex at about 870 ms. Forward modelling of various waves from the source to given receivers suggested that this event was a refracting, source generated shear wave. The shear wave velocities used were determined from the P wave velocities with V_p/V_s ratios of 2.4 in the near surface and 2.2 for the rest of the section. Ray trace modelling and the calculated synthetics are shown in Figures 12 and 13. While the shear wave events in this data set are of considerable interest, and perhaps surprise, their thorough analysis is outside the scope of this paper.

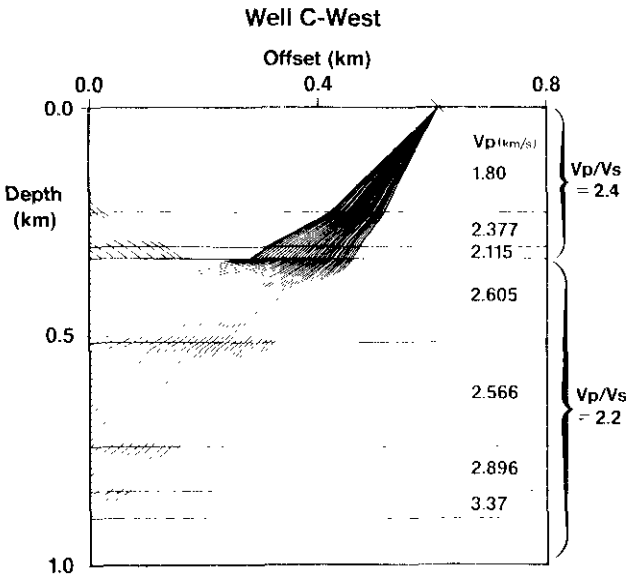

Fig. 12. Shear wave ray tracing for west VSP. Rays are traced through the velocity structure determined from the P wave velocities with Vp Vs ratios as shown

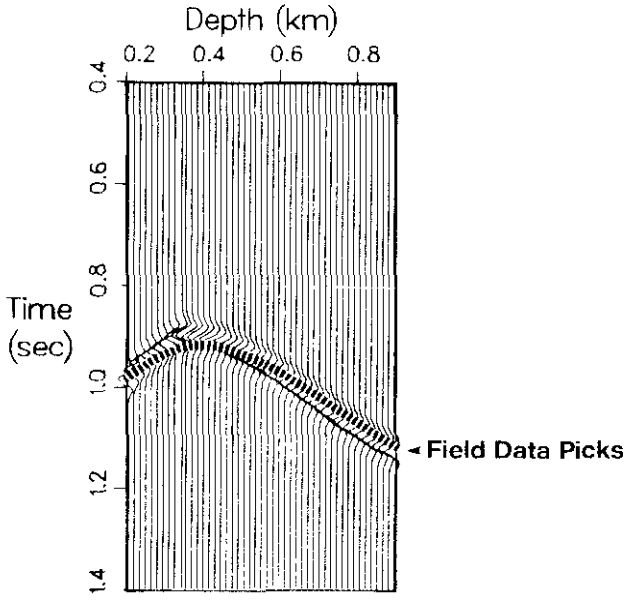

Fig. 13. Comparison of modelled shear wave arrivals with observed events from west offset VSP.

Well 3F had an 11 trace VSP acquired close to the bottom of the borehole. The small VSP was conventionally processed to give a deconvolved VSP extracted trace (VET). This VET is a two-way time, zero offset, normal incidence trace similar to the conventional surface seismic trace at the wellhead position. It can complement the synthetic seismogram as it extends below the bottom of the borehole and is a seismic (not sonic) measurement. The check shot survey in well C was also processed as a VSP. Note that the use of median filters makes unnecessary the spatial sampling criteria used in f/k filtering. This can allow processing of check shot surveys as VSP data. The result of this check shot processing is a check shot extracted trace (CET — the poor man's VET). Even with the few levels used in these surveys, good extracted traces were acquired. These traces are displayed in Figure 14. The major events of interests are reasonably consistent for the two extracted traces.

Note the Glauconite trough at about 770 ms, the Mississippian event at 822 ms and the Wabamun at around 885 ms.

Well F2 had a complete zero offset VSP acquired (Fig. 6). This VSP was also processed in a conventional manner to produce a VSP extracted trace. Because the propagating source wavelet in the VSP is measured (the downgoing wave), it is possible to deterministically deconvolve the upgoing waves. This allows a deconvolution to shape the upgoing reflection data to a known phase (*e.g.* zero phase). In this case, a sparse-spike deconvolution procedure was used (Chi *et al.*, 1984). The resultant sparse spike trace from well F2 is also shown in Figure 14. This current sparse spike series shows a high degree of similarity to the other trace sets. The amplitude of the traces has not been normalized in Figure 14. One important use of this spike series is to determine and shape the phase of the corresponding surface seismic. Because of the reasonable consistency in borehole data and the desire to make the seismic data a reasonably well-known (zero) phase, a shaping filter was designed to match the CDP data at the borehole with the check shot extracted trace. The result of wave shaping the CDP data to the check shot extracted trace is shown in Figure 15. Several observations were made. First, the interpreters of this section felt that the Mississippian reflection had been enhanced and showed a more distinct topography. Furthermore, the Glauconite event around Well C displayed some evidence of faulting. This faulting would be consistent with geologic and engineering data in the region. Third and perhaps most important, the original surface seismic data were about 90° out of phase with the VSP data. Further comparisons with synthetic seismograms and other VSP data gave consistent results that the original surface seismic sections (processed prior to this work) were 90° out of phase with the VSP and well-log data. It was later discovered that all of these previously processed sections had been rotated by 90°.

Velocities below the bottom of the borehole were also determined using the maximum-likelihood inversion technique (Hampson and Russell, 1985) on the separated upgoing and downgoing VSP data from the

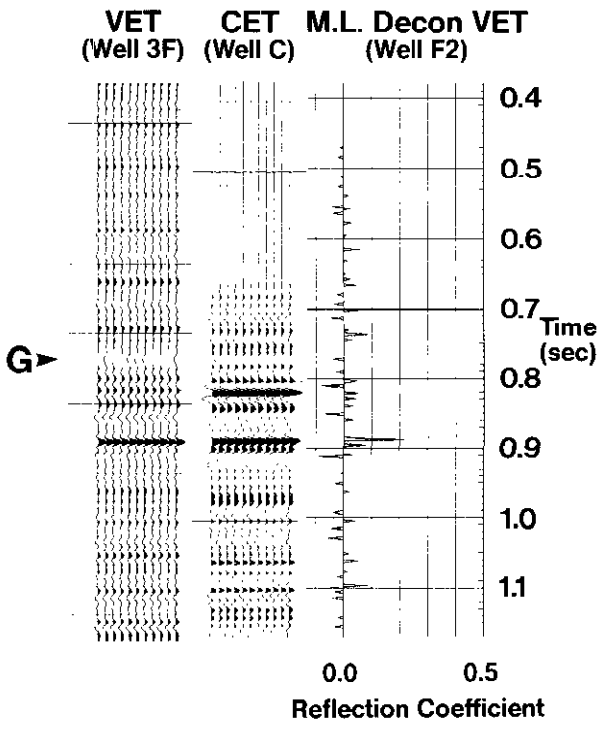

Fig. 14. Comparison of the traces extracted from well 3F VSP survey, well C check shot survey and the maximum-likelihood, sparse spike deconvolved, VSP trace extracted from the well F2 survey. The arrow shows the event time of the Glauconitic sand.

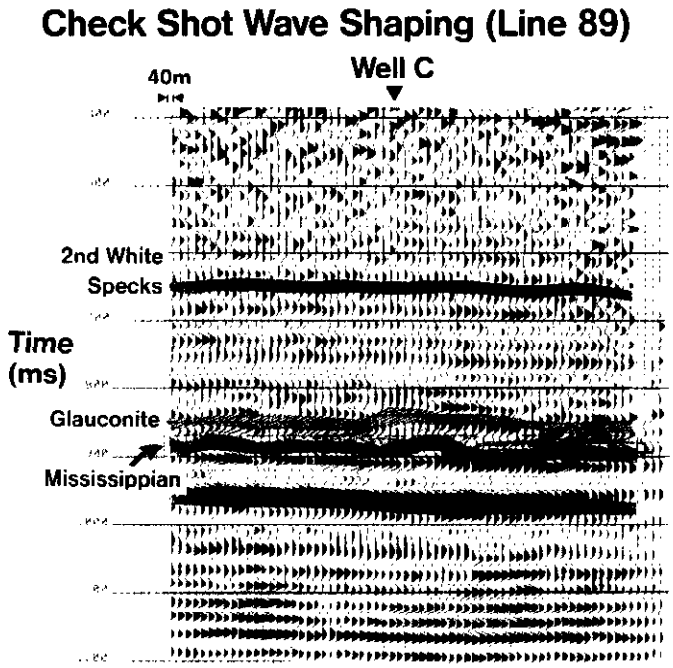

Fig. 15. Seismic section (line 89) shaped to the check shot extracted trace at well C.

well F2 survey. This analysis is generally called "prediction ahead of the bit" and involves converting the reflection spikes shown in Figure 14 to a velocity log. These velocities as well as those from the first-break traveltime inversion were used in the VSPCDP map processes (Wyatt and Wyatt, 1984; Dillon and Thomson, 1984), for east and west VSP surveys in well C. The processing flow for the VSP imaging was fairly standard (Hardage, 1983; Balch and Lee, 1984). In overview the downgoing waves are aligned, then enhanced via median filtering. These enhanced downgoing waves are subtracted from the total data. The resultant upgoing waves are then stretched into two-way time using an NMO-type algorithm. Noise is rejected at this stage by using various combinations of f/k filtering, stochastic tau-p filtering (Hampson and Dunham, 1985) and median f/k filtering (Stewart, 1985b). These enhanced upgoing data are then mapped laterally via a VSPCDP map process. The merged east and west VSP sections processed as above are shown in Figure 16. The sandstone of interest is evidence on this section at about 850 ms on the zero offset trace. Note that there is about a 5 ms dip in the Glauconite in the region of well C from west to east (left to right). This time shift corresponds to structure of about 7 m as compared with that from the well logs of about 5 m. The top of the Mississippian trends from about 887 ms on the left of Figure 16 to 900 ms on the right of the figure. The Wabamun event shows a slight dip to the east. The eastern VSP section is of poorer quality than the west. This is partially due to the more limited vertical extent of data acquired (Fig. 5) which gives rise to a more restricted and lower-fold lateral image.

Conventional processing of the 3-D seismic shot in the area provided sections such as line 88 shown in Figure 17. The 3-D seismic reprocessing did not include a 90° phase rotation as discussed previously. This E-W line crossed the apex of the sandstone at CDP 8840, near which the wells of interest were drilled. Again the top of Glauconite sandstone is evidence at about 850 ms. Further enhanced 3-D seismic processing (discussed in the next section) was performed by using VSP and well-log data in a tomographic scheme.

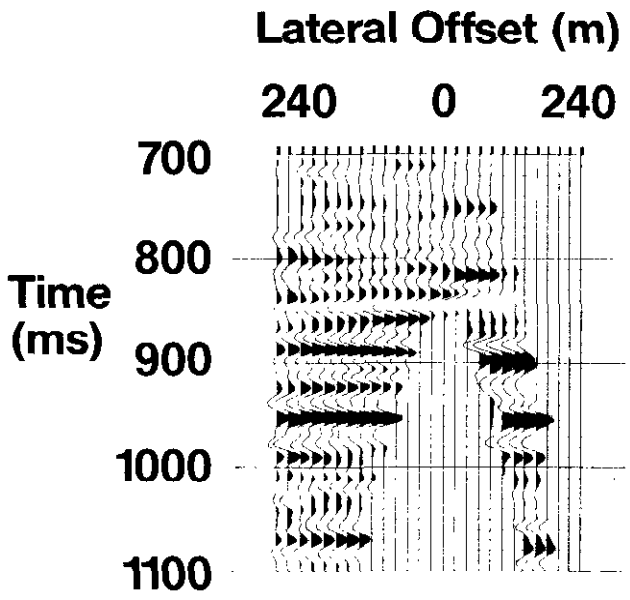

Fig. 16. Processed VSP sections (east and west merged) around Well C. The top of the Mississippian and Wabamun (lower) strata at 890 ms and 950 ms respectively.

Tomographic Technique

The previous sections have briefly discussed various geophysical data sets acquired and interpreted in this area. Instead of processing the data sets separately (and interpreting by, for example, sliding various stretched synthetic seismograms and well-logs up and down the seismic sections), we will discuss a method of coupling the measurements in one analysis. A tomographic technique has been developed to obtain a two- or three-dimensional velocity structure of the subsurface from observations of surface seismic and/or VSP and well-log data. The technique is basically a traveltime inversion (Aki and Lee, 1976; Lines *et al.*, 1984; Stewart, 1984; Chiu *et al.*, 1986; Stewart and Chiu, 1986). It uses direct and reflected events on the VSP, reflected events picked from the pre-stack 3-D seismic data and the depths of events (lithologic boundaries) at the well from

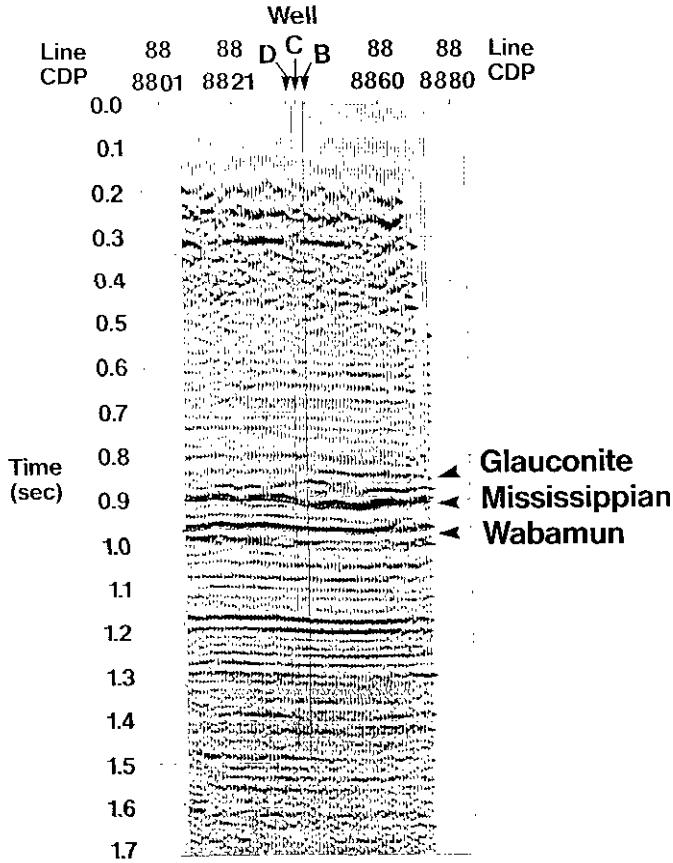

Fig. 17. Seismic section (Line 88) from the 3-D set. This E-W surface seismic line is located 40 m to the north of well C.

the well-logs. Rays are traced from the surface source locations to their associated receivers through a proposed model or medium. The medium consists of continuous curved interfaces defined by polynomials (or sinusoidal superpositions) separating regions of constant isotropic or transversely isotropic velocity. Ray tracing for each source-receiver pair is determined by solving a system of nonlinear equations for the minimum traveltime ray path (Chander, 1977). The intial model is guessed from knowledge of interfaces from the well-logs and VSP reflections as well as the preprocessed surface seismic data. A least-squares formulation (with singular value decomposition) is used to update the model by minimizing the difference between the observations and computed traveltimes. Updating iterations continue until the convergence criteria are met (that is, until the parameters or the traveltime residual are changing insignificantly).

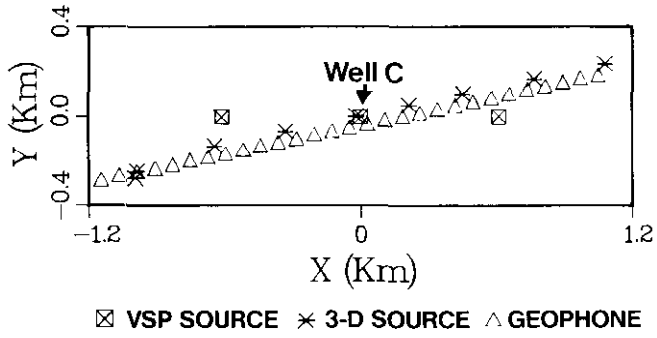

Fig. 18. Shot/receiver geometry for portions of the 3-D seismic data set used in the tomographic inversion.

The shot/receiver geometry of the 3-D surface seismic used in the tomographic inversion is shown in Figure 18. Three events were picked from deconvolved shot gathers similar to the one shown in Figure 19. The events are picked, using an interactive PC-based program. These events are subsequently input into the tomographic routines. These three events were associated with the top of the Glauconite, Mississippian unconformity and Wabamun. Considerable care was involved in interpreting the events and picking the three events on each trace. The first breaks from the two VSP surveys and check shots were also picked as previously mentioned.

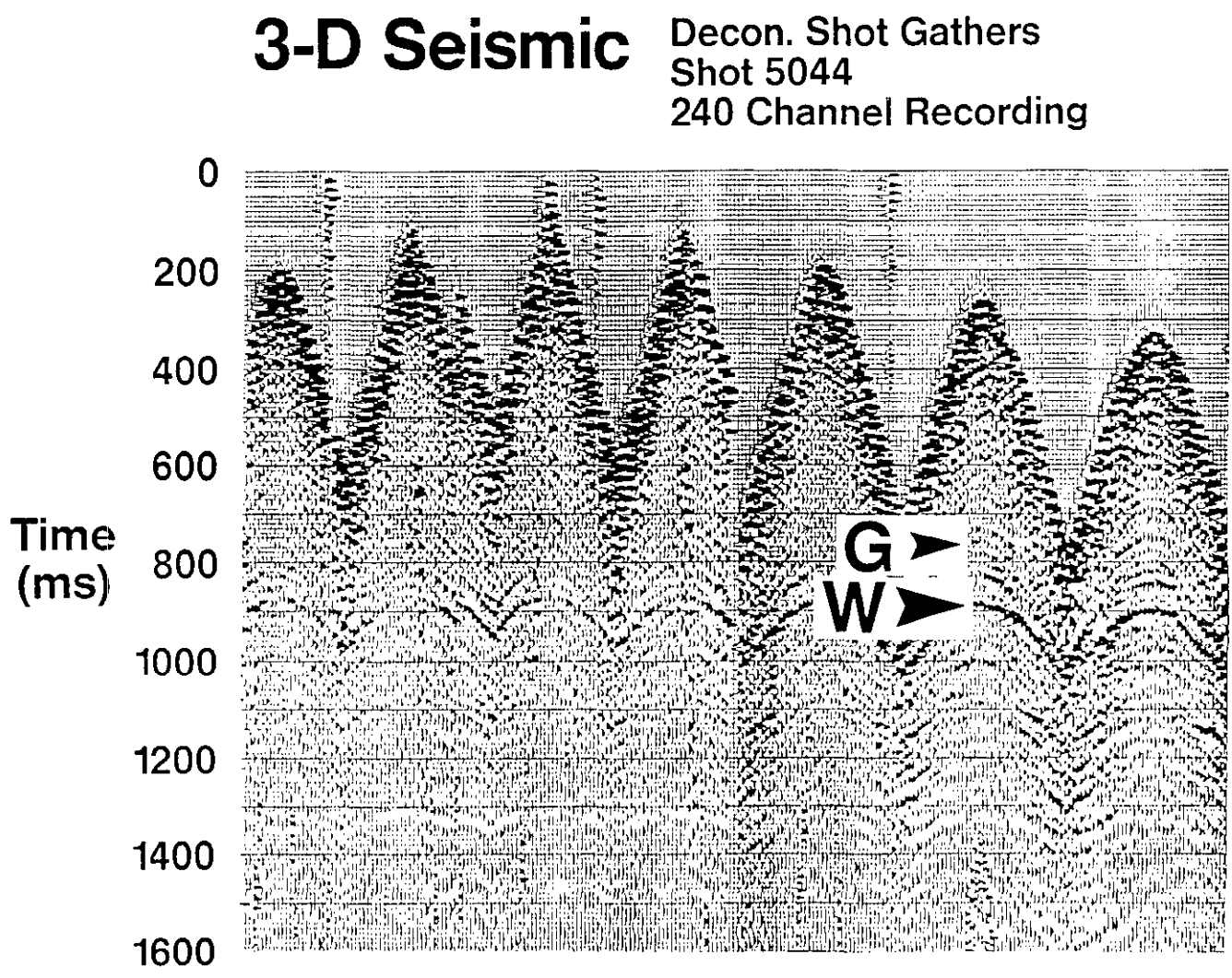

Fig. 19. Single deconvolved shot gather from the 3-D seismic survey for a shot near well C. The Glauconitic sandstone and Wabamun are annotated

as well as a number of reflected events on the two offset VSP sections. For reasons concerning anisotropy, discussed later, events that had angles of incidence greater than about 35 degrees from the vertical were not used in the inversion. All of the above angle-limited data were entered into the 3-D inversion algorithm. Note also that while the survey geometries were three-dimensional, the model used was constant in the off line (y) direction. A 3-D model can be used in the inversion algorithm but, as the data used in this discussion (Fig. 18) were largely in line, only a 2-D model is considered. This is likely a reasonable approximation as the logs (Fig. 7) in the offline direction show only a several metre dip across a lateral distance of about 400 m. As discussed previously, the algorithm ray traces through a given model, then compares the calculated traveltimes with the observed times. The model velocities and interfaces are updated in a manner to minimize the difference between observations and calculations. The tomography code is currently operating on a MicroVAX II computer. An inversion, as the one described here, requires about 25 minutes of CPU time.

Selected rays reflecting from the top of the Glauconite are shown in Figure 20. A cross-section of the final inversion model is shown in Figure 21. An important aspect of this model is that it is in depth. The tomographic velocity profile at the well C location is compared with the neighbouring sonic log from well F2 in Figure 21 (recall that there was no sonic log for well C). The tomographic velocity is fairly similar to the sonic log but with slightly lower velocities. This is expected due to velocity dispersion (Stewart *et al.*, 1984). If more layers had been used in the tomographic inversion the blocky nature of the sonic log could have been matched more closely.

This tomographic velocity (least-squares consistent with log and seismic measurements) is the sparse seismic representation of the geology of this region, in depth. It can be used on its own for contouring and interpretation, or employed in a number of ways to enhance the 3-D seismic data processing and interpretation. One of its first applications here is to map the conventional time-migrated section into depth. The result of this mapping or stretching is shown in Figure 22. Detailed mapping of the top of the Glauconite can now be performed. Note that this depth section predicts maximum topographic variation across the top of the Glauconite of about 15 m. Also the top of the Glauconite changes by about 5 m from well D to well B. The details of this relief on the Glauconite are consistent with the density logs shown in Figure 8. The sub-sea Glauconite top map, shown in Figure 3, used interval velocities determined from the correlation of interpreted seismic events in time with the depths of the corresponding formations on the well logs. These velocities were used to stretch the seismic time sections into depth. This process appears to overestimate the Glauconite topography, as it predicts Glauconite relief of about 12 m from well D to well B (as opposed to 5 m from the well-logs and tomography). Also total relief on the sub-sea depth map from the left of the map to well B is

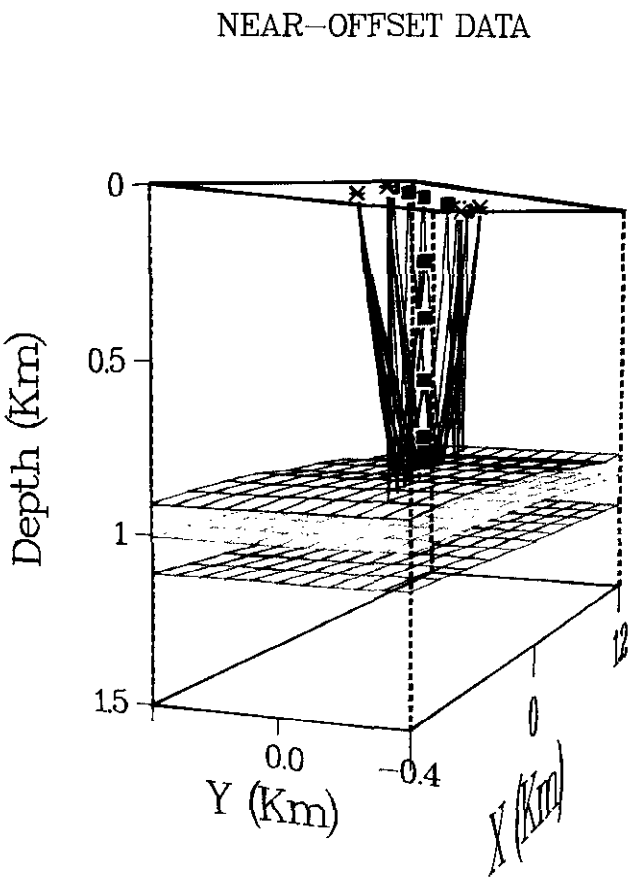

Fig. 20. Ray tracing between selected source and receiver positions for rays which reflect from the top of the Glauconite.

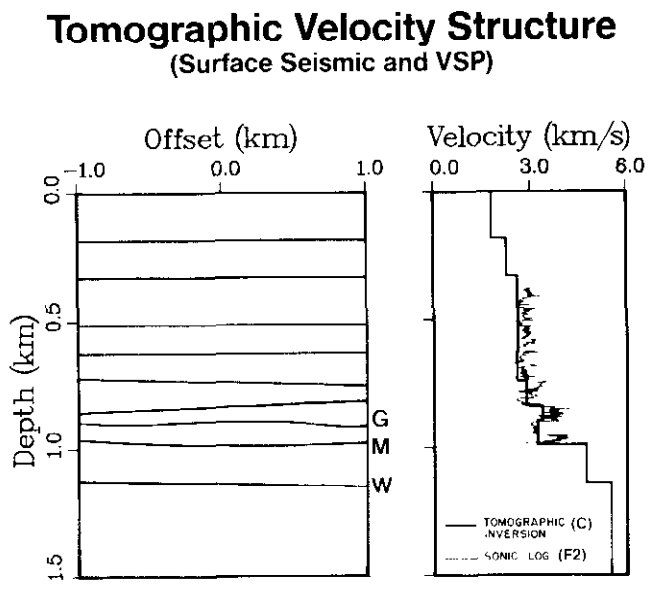

Fig. 21. Velocity structure in depth (on left) from tomographic inversion. On the right are the tomographic velocity log at zero offset and sonic log from well F2. Note that the seismic velocities are generally lower than the sonic velocities.

approximately 30 m. The tomographic depth section predicts a relief up to about 20 m. We do not know the reason for this discrepancy but it may be associated with anisotropy (Winterstein, 1986).

Let us return our attention to the time-migrated section (but now remigrated with the tomographic velocities). It is possible to perform "seismic inversion" on the time section. In this case, the reflection traces are converted to pseudo-sonic logs. This is done via the maximum-likelihood, sparse-spike deconvolution and inversion (Chi *et al.*, 1984; Hampson and Russell, 1985). In broad terms, the deconvolution picks a series of reflection coefficient spikes in the traces which, when convolved with an extracted wavelet, reproduce the original trace most accurately. The inversion converts the reflection coefficient to impedance or velocity steps, subject to a least-squares constraint of some background impedance or velocity profile. The impedance logs are converted to velocity logs, if density is not constant, using a calibrated empirical relationship (such as that of Gardner *et al.*, 1974, where impedance varies with velocity to the 5/4 power).

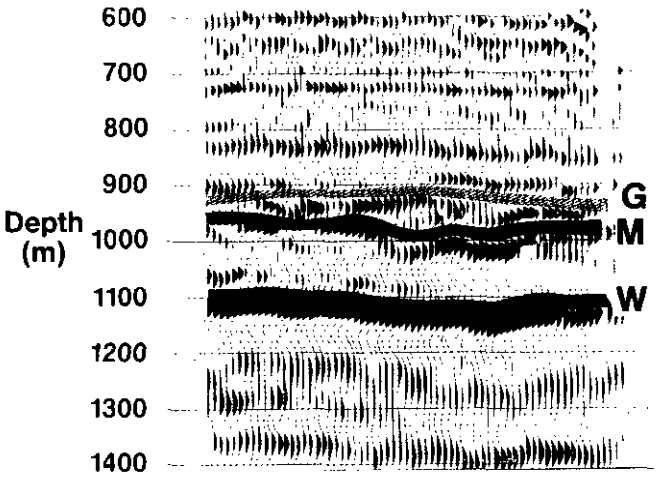

Fig. 22. Seismic depth section (line 89). The migrated time section has been stretched into depth using the tomographic velocity structure.

VSP data and tomographic velocities can make the inversion more accurate in two ways: i) the wavelet in the surface data can be estimated and shaped by comparison with the VSP extracted traces, ii) an accurate, low-frequency velocity constraint is provided by the tomographic analysis. After inversion, this pseudo-sonic section can be mapped into depth, again using the tomographic velocities. In the current case, the density was assumed to be constant, and the tomographic velocities were used as a constraint for the inversion. This resultant pseudo-sonic section in depth is shown in Figure 23. The pseudo-sonic section in depth is the

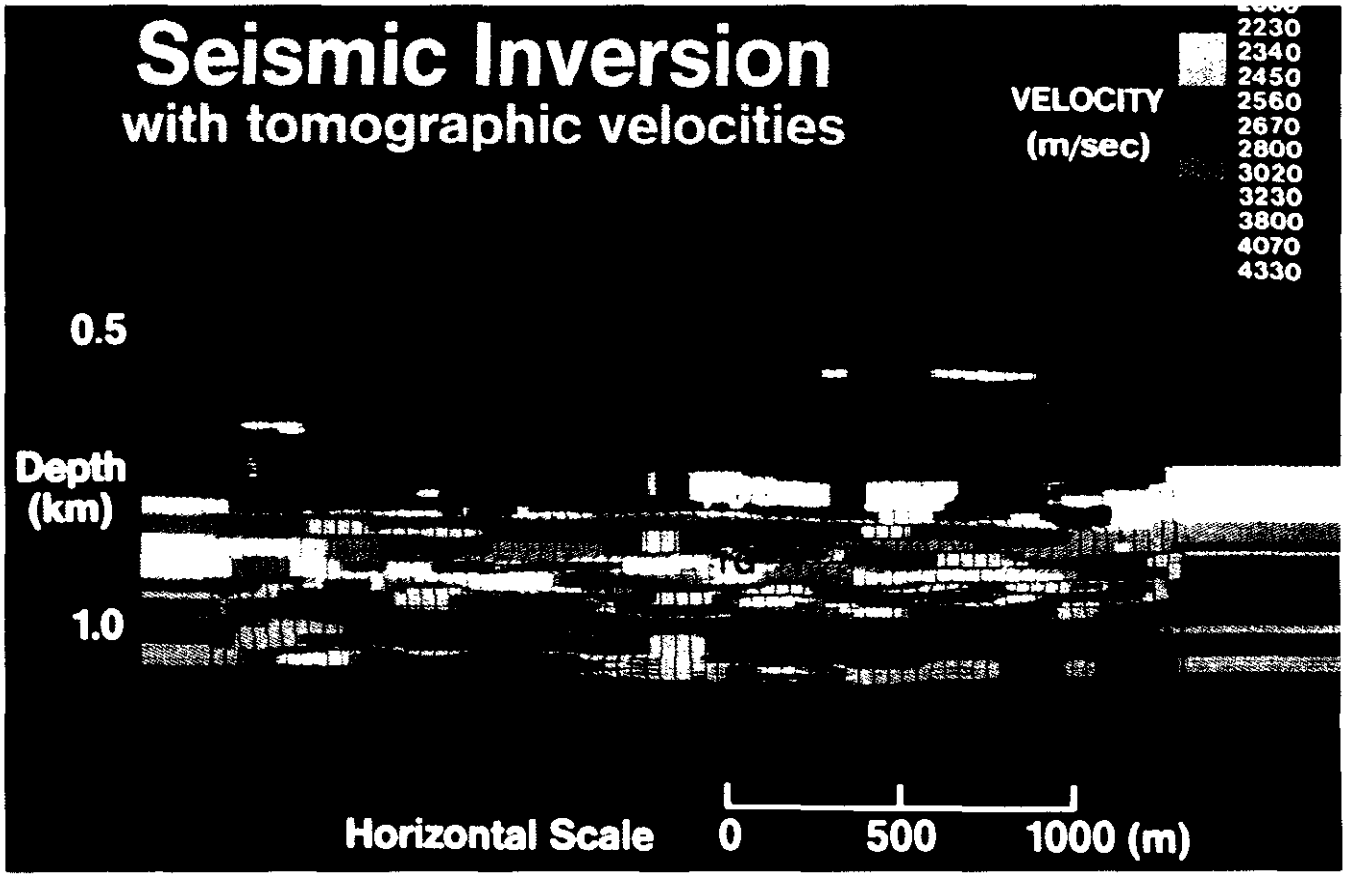

Fig. 23. Pseudo-sonic log section from the inversion of the time migrated section. Tomographic velocities are used as the constraint in the inversion process, then used to stretch the pseudo-sonic section in time to a section in depth.

main result that we wanted to achieve. It is significant because it:

i) simultaneously and optimally uses much of the geophysical data available

ii) provides a DEPTH section that can be interpreted on its own or used to enhance other seismic data processing

iii) produces a detailed velocity section that should be more closely related to lithology, because of the more accurate low spatial frequency velocity trend.

Anisotropy

In our initial coupled inversion of zero and far offset VSP data with surface seismic data, it was found that there were some sizable systematic traveltime residuals that were not reduced by further iteration. In general, the far offset VSP and large offset surface traveltimes did not agree with the modelled small offset surface and VSP data. Thus in the inversions used this far, offsets were limited such that reflection angles were less than about 35°. The traces corresponding to this angle of incidence were inferred via ray tracing through a preliminary model, for various source-receiver geometries. These limited angle inversions provided a solution with smaller time residuals. Inverting the far offset data alone also provided an independent, similar solution but with higher near-surface velocities.

To investigate briefly the possibility of an angle-dependent velocity, check shot, VSP and first-break refractions were analyzed. We assumed P wave transverse isotropy — that is, the medium layers are characterized by vertical and horizontal P wave velocities with elliptical velocity dependence on incidence angle. A two-layer near-surface model was proposed with two fixed layers — the first to 185 m and second to 365 m. Our ray tracing code was re-written to assume transverse isotropy where the generalized Snell's law holds (Levin, 1978; Crampin *et al.*, 1982; Gaiser *et al.*, 1984b; Chiu and Stewart, 1986). We call the ratio of horizontal velocity to vertical velocity, the anisotropy factor. Because only the check shot had an observation at 185 m, which gave a vertical velocity of 1785 m/s, this was kept constant in all the inversions.

The check shot vertical velocity for the second layer is 2265 m/s. The anisotropic inversion of the west VSP traveltimes alone gave vertical and horizontal velocities in the second layer of 2304 m/s and 2707 m/s. This implies an anistropy factor of 1.17.

The refracted first-arrival breaks in the surface data, with locations shown in Figure 18, were also inverted to provide a horizontal velocity in the second layer. The horizontal velocity determined from this refraction analysis is 2696 m/s. Thus the horizontal velocities from the VSP data and refraction data agree quite closely.

Simultaneous inversion of all the above data estimated an anisotropy factor of 1.18. That is, horizontal velocities are 18% higher than vertical velocities. All of these results suggest that anisotropy, at least in the near surface, is significant and needs to be accounted for in offset seismic data analysis.

Discussion and Future Work

As actual geology is in depth, not two-way time, and wells are also drilled in depth and not two-way time, it is compelling to process seismic data into a depth image. This has not been the standard processing result in times past. Perhaps this is partially because the velocity structure was not very accurate and thus the basic conversion of observed seismic times to depth gave sections that tied poorly to the well-logs. However, with greater understanding of well-logs (especially sonic logs) plus the acquisition and use of VSP and anisotropy, accurate seismic interval velocities in depth can be found. A more precise velocity in depth (especially a 2-or 3-D tomographic velocity) can provide the basis for depth sections that are perhaps more directly relevant to the lithology.

A time migration and depth stretch was used in this study, as opposed to a depth migration, to facilitate use of the maximum-likelihood deconvolution and inversion. Deconvolution operates in the time domain as does the inversion applied, so migration was done prior to time-to-depth conversion. Again the final goal was to provide a blocky (sparse) pseudo-sonic in depth. However, it would be interesting to depth-migrate the data and compare the depth migration to the time migration and time-to-depth stretch. It would also be of interest to perform seismic inversion on the depth-migrated section and compare that with the blocky inversion stretched to depth.

In this work, we have used only a small number of the 3-D seismic shots. It is straightforward, but time-consuming, to pick more of the surface seismic data and invert for a full 3-D subsurface sparse geologic model. Currently, under development is an automatic picking algorithm for 3-D seismic gathers. This will facilitate the inputting of large numbers of traveltime picks which can be inverted for 3-D velocity structure. Full waveform methods of tomography that can bypass the traveltime picking stage will undoubtedly be given greater attention in the future.

Another limitation in the current tomographic inverse software is that while the subsurface model interfaces are three-dimensional, the intervening layers have constant velocities. This allows rapid ray tracing but may not be realistic geologically. To give the inversion process the capability of estimating lateral velocity variation, we are in the process of hybridizing the inversion code. This is being accomplished by first estimating the model from the traveltime inverse, then pixelating (superimposing squares on) the layers. The traveltime residuals (difference between the observed and calculated traveltimes) are used in an Algebraic Reconstruction Technique (ART) to estimate the lateral changes in

the pixels superimposed on the initial estimated structure. Via this pixel estimation and residual subtraction, an iterative inversion that estimates structure and lateral velocity variation can be achieved.

CONCLUSIONS

A thorough suite of geophysical measurements has been acquired over a producing, heavy oil development area. Conventional processing of well-log, VSP and 3-D seismic data allows an interpretation of the region near the Glauconitic sandstone reservoir and surrounding area. The VSP section provides an additional and consistent image of the reservoir structure and stratigraphy near the well. By using a tomographic technique (traveltime inversion), further interpretation of the region can be made by integrating well-log, VSP and 3-D seismic data into a velocity structure. This velocity structure forms the basis for time migration of the seismic data, seismic inversion of the section into pseudo-sonic logs and stretching of the pseudo-sonic section into depth. The seismic section in depth and pseudo-sonic section in depth have Glauconite topographies that are consistent with the wells drilled in the area. A previous Glauconite top map, prepared from well logs and interpreted seismic events only, appears to give an overestimate of the topography. A great deal yet remains to be understood about seismic velocity and images of the earth in depth. However, the coupling of geophysical measurements, via seismic tomography, holds considerable promise to increase our knowledge of the subsurface.

REFERENCES

Aki, K. and Lee, W.H., 1976, Determination of three dimensional velocity anomalies under a seismic array using first P arrivals from local earthquakes: Journal of Geophysical Research, v. 81, p. 4381-4399.

Anderson, D.L. and Dziewonski, A.M., 1984, Seismic tomography: Scientific American: v. 251, p. 60-68.

Balch, A.H. and Lee, M.W., 1984, Vertical Seismic Profiling: Technique, Applications and Case Histories: Boston, IHRDC Publishers.

Bishop, T.N., Bube, K.P., Cutler, R.T., Langan, R.T., Love, P.L., Resnick, J.R., Shuey, R.T., Spindler, D.A. and Wyld, H.W., 1985, Tomographic determination of velocity and depth in laterally varying media: Geophysics, v. 50, p. 6, 903-923.

Bois, P., LaPorte, M., Lavergne, M. and Thomas, G., 1972, Well-to-well seismic measurements: Geophysics, v. 37, p. 471-480.

Bregman, N.D., 1986, Tomographic Inversion of Crosshole Seismic Data: Ph.D. Thesis, University of Toronto.

Censor, Y., 1983, Finite series-expansion reconstruction methods: Proceedings IEEE, v. 71, p. 409-419.

Chander, R., 1977, On tracing seismic rays with specified end points in layers of constant velocity and plane interfaces: Geophysical Prospecting, v. 25, p. 120-124.

Chi, C., Mendel, J.M. and Hampson, D., 1984, A computationally fast approach to maximum-likelihood deconvolution: Geophysics, v. 49, p. 550-565.

Chiu, S.K.L., Kanasewich, E.R. and Phadke, 1986, 3-D determination of structure and velocity by seismic tomography: Geophysics, v. 51, p. 1559-1571.

_____ and Stewart, R.R., 1986, Tomographic determination of 3-D seismic velocity structure using well-log, VSP and surface seismic data: Geophysics (*in press*).

Crampin, S., Stephen, R.A. and McGonigle, R., 1982, The polarization of P-waves in anisotropic Media: Geophysical Journal, Royal Astronomical Society, v. 68, p. 477-485.

Devaney, A.J., 1984, Geophysical diffraction tomography: IEEE Transactions, Geoscience and Remote Sensing, v. GE-22, p. 3-13.

Dillon, P.B. and Thomson, R.C., 1984, Offset source VSP surveys and their image reconstruction: Geophysical Prospecting, v. 32, p. 790-811.

Dines, K.A. and Lytle, R.J., 1979, Computerized geophysical tomography: Proceedings, IEEE, v. 67, p. 1065-1073.

Gaiser, J.E., DiSiena, J.P. and Fix, J.E., 1984a, Vertical seismic profiles: fundamentals of the downgoing wavefield and applications that improve CDP data interpretation. *In*: Toksoz, M.N. and Stewart, R.R. (Eds.), Vertical Seismic Profiling, Part B: Advanced Concepts. Amsterdam, Geophysical Press.

_____, Ward, R.W. and DiSiena, J.P., 1984b, Three-component vertical seismic profiles: velocity anisotropy estimates from P wave particle motion. *In*: Toksoz, M.N. and Stewart, R.R. (Eds.), Vertical Seismic Profiling, Part B: Advanced Concepts. Amsterdam, Geophysical Press.

Gardner, G.H.F., Gardner, L.W. and Gregory, A.R., 1974, Formation velocity and density — the diagnostic basics of stratigraphic traps: Geophysics, v. 39, p. 770-780.

Hampson, D. and Dunham, A., 1985, Inverse velocity stacking for multiple suppression (abstract no. SP-5): National Canadian SEG Meeting, Calgary, Alberta, May 7-10.

_____ and Russell, B., 1985, Maximum-likelihood seismic inversion (abstract no. SP-16): National Canadian SEG Meeting, Calgary, Alberta, May 7-10.

Hardage, B.A., 1983, Vertical Seismic Profiling, Part A: Principles: Amsterdam, Geophysical Press.

Levin, F.K., 1978, The Reflection, refraction and diffraction of waves in media with an elliptical velocity dependence: Geophysics, v. 43, p. 528-537.

Lines, L.R., Bourgeois, A. and Covey, J.D., 1984, Traveltime inversion of vertical seismic profiles — a feasibility study: Geophysics, v. 49, p. 250-264.

Louis, A.K. and Natterer, F., 1983, Mathematical problems of computerized tomography: Proceedings, IEEE, v. 71, p. 379-389.

Mason, I.M., 1981, Algebraic reconstruction of a two-dimensional *velocity inhomogeneity in the high Hazles seam of Thoresby Colliery*: Geophysics, v. 46, p. 298-308.

McMechan, G.A., 1983, Seismic tomography in boreholes: Geophysical Journal of the Royal Astronomical Society, v. 74, p. 601-612.

Morgan, C.L., 1983, Basic Principles of Computed Tomography: Baltimore, University Park Press.

Omnes, G., 1984, Deconvolution of Surface Seismic Trade Using VSP Data. *In*: Toksoz, M.N. and Stewart, R.R. (Eds.), Vertical Seismic Profiling, Part B: Advanced Concepts. Amsterdam, Geophysical Press.

Peterson, J.E., Paulsson, B.N. and McEvilly, T.N., 1985, Applications of algebraic reconstruction techniques to crosshold data: Geophysics, v. 50, p. 1566-1580.

Pullin, N.E., Matthews, L.W. and Hirsche, W.K., 1986, Techniques applied to obtain very high resolution 3-D seismic imaging at an Athabasca Tar Sands thermal pilot project (abstract no. 3D-6): National Canadian SEG Meeting, Calgary, Alberta, May 7-10.

Roth, K., 1984, NMR — Tomography and Spectroscopy in Medicine: An Introduction: Berlin, Springer-Verlag.

Seeram, E., 1982, Computed Tomography Technology: Philadelphia, W.B. Saunders Co.

Stewart, R.R., 1984, VSP interval velocities from traveltime inversion: Geophysical Prospecting, v. 32, p. 608-628.

_____, Huddleston, P.D. and Kan, T.K., 1984, Seismic versus sonic velocities: a VSP study: Geophysics, v. 49, p. 1153-1168.

_____, 1985a, Seismic tomography: Pursuing a better subsurface picture: Oilweek, v. 36, no. 35.

_____, 1985b, Median filtering: review and a new F/K analogue design: Journal of the Canadian Society of Exploration Geophysicists, v. 21, p. 54-63.

_____ and Chiu, S.K.L., 1986, Seismic tomographic imaging applied to a Glauconitic Sandstone development area (abstract, no. CAS-11): National Canadian SEG Meeting, Calgary, Alberta, May 13-15.

Stork, C. and Clayton, R.W., 1985, Iterative tomographic and migration reconstruction of seismic images (abstract no. S19.3): 55th Annual International SEG Meeting, Oct. 6-10, Washington, D.C.

Taylor, G., 1984, Seismic resolution and field design: success and failure in Taber, Alberta, 1984: Journal of the Canadian Society of Exploration Geophysicists, v. 20, p. 7-22.

Tilley, B.J. and Longstaffe, F.J., 1984, Controls on hydrocarbon accumulation in Glauconitic Sandstone, Suffield Heavy Oil Sands, southern Alberta: American Association of Petroleum Geologists Bulletin, v. 68, p. 1004-1023.

Winterstein, D.F., 1986, Anisotropy effects in P-wave and SH-wave stacking velocities contain information on lithology: Geophysics, v. 51, p. 661-672.

Wong, J., Hurley, P. and West, G.F., 1983, Crosshole seismology and seismic imaging in crystalline rocks: Geophysical Research Letters, v. 10, p. 686-689.

Worthington, M.H., 1984, An introduction to geophysical tomography: First Break, v. 2, no. 11, p. 20-26.

Wyatt, K.B. and Wyatt, S.B., 1984, Determining subsurface structure using the vertical seismic profile: *In*: Toksoz, M.N. and Stewart, R.R. (Eds.), vertical seismic profiling, Part B: Advanced Concepts. Amsterdam, Geophysical Press.